

RISER RESPONSE TO DIRECTIONAL SEAS

A Thesis

by

GERARD LEWIS MCCOY III

Submitted to the Graduate College of
Texas A&M University
in partial fulfillment of the requirements for the degree of

MASTER OF SCIENCE

August 1985

Major Subject: Ocean Engineering

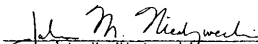
RISER RESPONSE TO DIRECTIONAL SEAS


A Thesis

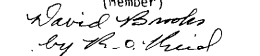
by

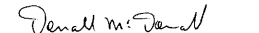
GERARD LEWIS MCCOY III

Approved as to style and content by:


John M. Niedzwecki
(Chair of Committee)


H. K. Lou
(Member)


David A. Brooks
(Member)


Donald McDonald
(Head of Department)

August 1985

ABSTRACT

Riser Response to Directional Seas. (August 1985)

Gerard Lewis McCoy III, B.S., Texas A & M University

Chairman of Advisory Committee: Dr. John M. Niedzwecki

This thesis examines the dynamic response of a coupled vessel/riser system to directional seas. The introduction of directional seas into the analysis provides a truer representation than unidirectional sea conditions and reduces the overdesign typical of riser analyses.

A planar riser model is developed to calculate displacements and stresses, the solution being performed in the frequency domain using finite element methods. Model verification is provided through a direct comparison with an API bulletin on marine risers.

Inherent in the frequency domain solution is the assumption of linearity. The drag force term, being non-linear, requires linearization. Two linearization methods will be compared to find the effects on displacements and stresses.

Recent findings have indicated the importance of vessel motion on riser dynamics. Effects of vessel phasing on displacements and stresses are compared and discussed.

The directional displacements and stresses are calculated for a low energy sea and a storm sea. The magnitude of directional spreading is varied in order to ascertain the effects of degree of

directional spread. The response characteristics of a cylindrical floating platform and a typical drillship are compared. The use of a directional sea is found to decrease maximum displacements and stresses along the riser. With this knowledge available riser overdesign can be minimized.

ACKNOWLEDGEMENT

I would like to thank my wife, Lisa, whose support and patience throughout these last few years made everything much easier for me. She drew the figures contained in the thesis and as a result of her super job the quality of the thesis is enhanced.

I would like to express my sincere gratitude to Dr. John M. Niedzwecki. He provided great guidance throughout and very willingly spent many hours of his own time helping me. The motivational "butt-kicking" received on occasion was never appreciated at the time of occurrence but in retrospect proved to be some of the best "advice" offered.

I am greatly indebted to Dr. Y. K. Lou and Dr. David Brooks for their expertise and support. Special thanks is extended to Dr. Robert Reid for substituting at my defense in place of Dr. David Brooks.

My undergraduate education was provided for by my parents and I would like to thank them. The education I received provided me with the ability to continue on to graduate school while being self-supportive.

Gerard L. McCoy III

August, 1985

TABLE OF CONTENTS

	Page
ABSTRACT.	iii
ACKNOWLEDGEMENT	v
TABLE OF CONTENTS	vi
LIST OF TABLES.	viii
LIST OF FIGURES	ix
I. INTRODUCTION.	1
II. DEVELOPMENT OF THE MATHEMATICAL AND NUMERICAL MODELS.	10
Finite Element Representation	10
Mass Matrix	12
Stiffness Matrix.	12
Damping Matrix.	13
Eigen Analysis.	14
Current and Wave Forces	15
Borgman Linearization Procedure	16
Krolikowsky and Gay Linearization Procedure	18
Directional Seas.	21
Responses and Numerical Procedures.	26
Basic Procedure	26
Directional Response Considerations	30
III. NUMERICAL RESULTS	35
Comparison With API Codes	35
Vessel Phasing Comparison Cases	42

TABLE OF CONTENTS(continued)

Linearization Method Comparison Cases	46
Directional Sea Responses	50
IV. SUMMARY AND CONCLUSIONS	62
REFERENCES.	66
APPENDIX. NOMENCLATURE	68
VITA.	72

LIST OF TABLES

Table	Page
1. References of Three Dimensional Dynamic Analyses.	6
2. Riser Properties.	36

LIST OF FIGURES

Figure	Page
1. Riser Response to a Unidirectional Wave	3
2. Riser Response to a Directional Sea	8
3. Directional Energy Spectrum	23
4. Displacement Ranges for API Comparison- 500 ft Depth.	37
5. Maximum Bending Stresses for API Comparison- 500 ft Depth	38
6. Displacement Ranges for API Comparison- 1500 ft Depth	40
7. Maximum Bending Stresses for API Comparison- 1500 ft Depth.	41
8. Displacement Ranges for Vessel Phasing Comparison	44
9. Maximum Bending Stresses for Vessel Phasing Comparison.	45
10. Maximum Displacements for Linearization Comparison.	48
11. Maximum Bending Stresses for Linearization Comparison	49
12. Vessel Response Amplitude Operators	52
13. Comparison of Spreading Concentration Factors	54
14. Displacements for Directional Seas- 20 Knots.	56
15. Bending Stresses for Directional Seas- 20 Knots	57
16. Displacements for Directional Seas- 40 Knots.	58
17. Bending Stresses for Directional Seas- 40 Knots	59

I. INTRODUCTION

Offshore oil and gas exploration has been occurring since the early twentieth century. Typical structures for those times were placed in water depths usually less than 50 feet. These structures were knowingly oversized since the offshore environmental forces were not well understood. In an effort to minimize overdesign, research into offshore environmental forces and structures able to withstand those forces was undertaken. With a better understanding of the offshore environment, structure design can be optimized so as to yield the most economical choice for the type situation to be encountered. Current oil and gas exploration is occurring or is planned for water depths approaching 5,000 feet. Fixed jacket structures, gravity platforms, and jack-up rigs are used in depths of up to 1,000 feet beyond which they become uneconomical to deploy. One of the most economical methods for oil and gas exploration beyond 300 feet of water is a drillship or floating platform coupled with a riser system.

A riser is best described as the structural link between the surface vessel and the seafloor. The surface vessel can be a drillship, semi-submersible, or possibly a tension leg platform. A telescoping pipe with a ball joint at the lower end is the top

The citations on the following pages follow the style of Ocean Engineering- An International Journal of Research and Development.

connection to the riser. The bottom of the riser is connected to a blow-out-preventer at the seafloor. A tensioner on the surface vessel is used to provide a tension to the riser. The surface vessel is constrained in surge and sway motions by either a dynamic positioning system or by mooring lines. Fig. 1 depicts a planar riser system responding to a unidirectional wave.

The numerical model of the riser is based upon theoretical considerations of a tensioned beam-column element. Finite element methods are used to take into account the lateral stiffness of the riser. The lateral stiffness of the riser is approximated by bending and geometric stiffness contributions. The mass distribution along the riser is accounted for through a lumped mass model which includes the steel mass, mud mass, and the effective added mass of the fluid. Hydrodynamic damping and equivalent viscous damping are taken into account. The viscous damping is assumed to be proportional to the mass and stiffness matrices in order to decouple the equations of motion. Damping ratios for each mode of vibration are given from which the equivalent viscous damping matrix is constructed.

The riser responds to the offshore environmental forces and the vessel motions. Morison's equation is used to transform the wave and current kinematics into forces acting on the riser system. Within the frequency domain solution lies the assumption of linearity; thus, the non-linear drag term in the wave force equation must be linearized. Two methods, one by Borgman(1969a) and one by Krolikowsky and Gay(1980), are currently available for this. Borgman(1969a) first

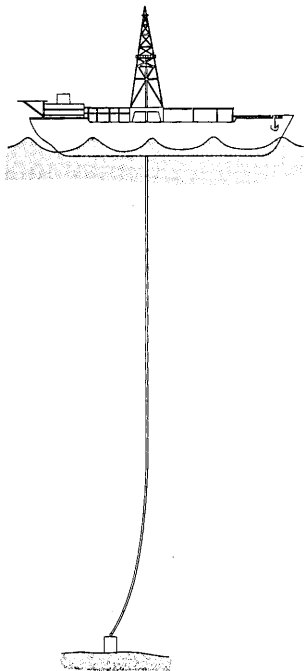


Fig. 1. Riser Response to a Unidirectional Wave

presented a linearization solution which provided the basis for most frequency domain riser analyses. He presented the method of equivalent linearization which minimizes the mean square error between the linearized approximation and the actual non-linear form. The method presented by Krolikowsky and Gay(1980) expands the drag force term in a Fourier series in order to minimize the mean square error. This method has not been incorporated in many riser analyses due to its recent development. The vessel motion effects are accounted for by forcing the riser's top end to respond as the vessel does, a dynamic boundary condition. Response amplitude operators are used to describe the vessel motion.

The unidirectional riser analysis is the standard analysis approach used by industry while few directional analyses are performed. Most riser response research has concentrated on planar responses due to unidirectional design waves. Chakrabarti and Frampton(1982) give an overview of many riser analyses previously published, the majority of which are unidirectional, planar analyses. The information summarized in their paper starts with the early project Mohole studies. The major conclusion which was stressed throughout the article was that a dynamic analysis is essential for deep water riser analyses. The frequency domain dynamic solution is used more often than the time history or random vibration solution. The frequency domain solution is used in this thesis.

Despite being the standard analysis approach used by industry, the unidirectional response does not represent the true response due

to short crested, confused seas. Difficulty with describing directional seas has been part of the problem. With recent advancements regarding directional sea kinematic descriptions it is possible to calculate directional responses.

Directional waves and corresponding wave kinematics can now be accurately described using a linear wave theory with an appropriate wave spreading function. Comparisons with field studies have confirmed this (Forristall et al., 1978). Accurate descriptions of wave kinematics were shown to be more dependent upon directionality than on the degree of non-linearity of the wave. What this means is that more accurate results are obtained using a linear wave theory with an appropriate spreading function as opposed to a unidirectional high order non-linear wave theory.

Due to the previous inability to describe directional sea conditions there has not been much literature published about directional riser responses. The few existing three-dimensional riser analyses focus on the methodology for treatment of the directional seas. Most papers reviewed, see Table 1, skirted the directional seas issue and studied orthogonal responses due to a resolved unidirectional wave. Gardner and Kotch (1976), Gnone et al. (1975), and Paulling (1975) have all completed three-dimensional riser response studies. All studies treat the wave force by the same method. Each chooses a unidirectional wave from which a wave force is calculated along the riser length. The force is then resolved into two orthogonal components. Responses in each orthogonal plane are then

Table 1. References of Three Dimensional Dynamic Analyses

Investigation	Dynamic Solution Type	Spatial Solution Technique	Wave Force Input
Gardner and Kotch(1976)	Time History	Finite Element	Resolved Unidirectional
Gnone, Signorelli, and Giuliano (1975)	Frequency Domain & Time History	Finite Element	Resolved Unidirectional
Paulling (1979)	Frequency Domain	Finite Element	Resolved Unidirectional
Berge and Penzien(1974)	Random Vibrations	not specified	Directional

calculated. The difficulty with this method lies in the treatment of the wave force. At best this method is an approximation to the directional wave force transmitted to the riser. Berge and Penzien(1974) calculate tower responses due to directional seas. The directional spectrum is calculated by separating the frequency-dependent parts from the directional-dependent parts. This allows use of an accepted spectral density with an appropriate spreading function. The Pierson-Moskowitz amplitude spectrum was used in conjunction with a circular normal spreading function. Although the method was applied to an offshore tower and not a riser, the basic approach is still applicable to riser problems.

The directional response of the riser is found by integration of various unidirectional responses around a mean wave direction. The wave kinematics in each direction are calculated using a linear wave theory with a spreading function. The unidirectional response for each direction is calculated based upon the wave kinematics for that direction. Fig. 2 depicts a directional riser response system.

The purpose of this thesis is to investigate riser response to directional seas. Directional seas allow a truer representation of the wave kinematics found in random short crested seas. Correspondingly, the wave forces and riser responses are more accurate. Thus, some aspects of overdesign may be minimized.

Differences between unidirectional and directional seas will be discussed. Typical design waves, usually from long period swell, do not exhibit as much directional spread as shorter period waves. Seas

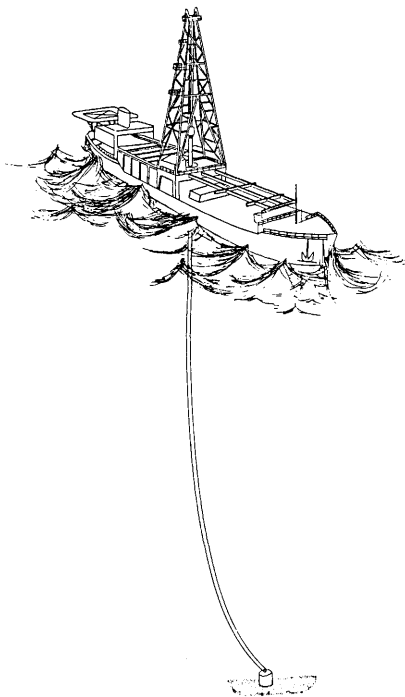


Fig. 2. Riser Response to a Directional Sea

of low energy content usually exhibit a large amount of directional spread; thus, the largest impact for directional seas representation is expected in the description of low energy seas.

Two drag force linearization methods will be discussed and results for each method will be compared. Since each method has the same motive, to match the actual non-linear drag form as closely as possible, the merits of each will be evident through a direct comparison.

The vessel motion effects on the riser response are seen to play an important role. The effects of vessel phasing with respect to the wave crest are to be investigated through comparisons using different values for the phasing angle.

II. DEVELOPMENT OF THE MATHEMATICAL AND NUMERICAL MODELS

This chapter contains the derivation of the planar riser motion equations. The finite element equations are calculated based upon the riser equations of motion. Once the elemental equations are known the eigen analysis is performed. Calculation of the current and wave forces is accomplished using two different linearization methods.

The directional sea spectrum is defined by a unidirectional wave spectrum in conjunction with a directional spreading function. Calculation of the directional responses due to a directional spectrum is possible once the unidirectional responses for different directions are known.

Finite Element Representation

Gardner and Kotch(1976) presented a derivation of the riser equation of motion based upon Bernoulli-Euler beam theory whereby lateral displacements are controlled primarily by bending and not shear. Only the results are presented here since the derivation is available in the article. The equilibrium equation can be expressed as

$$f = (m+m_a)\ddot{y} + EIy'''' - Ty'' - T'y' \quad (1)$$

where

$$T = T_0 + T'z \quad (2)$$

With the equilibrium equation known the total energy is available. The total energy of a uniform beam segment is the summation of the kinetic energy and the elastic strain energy,

$$KE + SE = \int_0^L \left[\frac{1}{2}(m+m_a)(\dot{y})^2 + \frac{1}{2}EI(y'')^2 + \frac{1}{2}(T_0+T'z)(y')^2 \right] dz . \quad (3)$$

The principle of stationarity of the total energy is used to obtain the finite element equations. The lateral displacement can be represented by the summation of four deformation functions known as the cubic Hermitian polynomials,

$$y = \sum_{i=1}^4 H_i y_i \quad (4)$$

where

$$H_1 = 1 - 3(z/L)^2 + 2(z/L)^3 , \quad (5a)$$

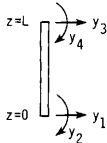
$$H_2 = z[1-(z/L)]^2 , \quad (5b)$$

$$H_3 = 3(z/L)^2 - 2(z/L)^3 , \quad (5c)$$

and

$$H_4 = \frac{z^2}{L} [(z/L) - 1] , \quad (5d)$$

for the configuration



Mass Matrix

A lumped mass formulation is used to represent the mass of the riser system. The assumption of zero rotational inertia provides a mass matrix with translational degrees of freedom only. With zero mass for the rotational modes the matrix becomes

$$[m]_{TOT} = \frac{(m + m_a)L}{2} \begin{bmatrix} 1 & 0 & 0 & 0 \\ 0 & 0 & 0 & 0 \\ 0 & 0 & 1 & 0 \\ 0 & 0 & 0 & 0 \end{bmatrix}. \quad (6)$$

Stiffness Matrix

The stiffness matrix is derived by applying the principle of minimization of strain energy,

$$k_{ij} = \frac{\partial^2 SE}{\partial y_i \partial y_j} = EI \int_0^L H_i' H_j' dz + T_0 \int_0^L H_i' H_j' dz + T' \int_0^L z H_i' H_j' dz. \quad (7)$$

where T_0 is the tension at the lower end of the element. The bending stiffness matrix so formed is

$$[k]_{EI} = \frac{2EI}{L^3} \begin{bmatrix} 6 & 3L & -6 & 3L \\ 3L & 2L^2 & -3L & L^2 \\ -6 & -3L & 6 & -3L \\ 3L & L^2 & -3L & 2L^2 \end{bmatrix}. \quad (8)$$

The initial constant tension stiffness matrix is

$$[k]_{T_0} = \frac{T_0}{30L} \begin{bmatrix} 36 & 3L & -36 & 3L \\ 3L & 4L^2 & -3L & -L^2 \\ -36 & -3L & 36 & -3L \\ 3L & -L^2 & -3L & 4L^2 \end{bmatrix}. \quad (9)$$

The varying tension stiffness matrix accounts for the linear variation of the tension along the element length,

$$[k]_{T'} = T' \begin{bmatrix} 3/5 & L/10 & -3/5 & 0 \\ L/10 & L^2/30 & -L/10 & -L^2/60 \\ -3/5 & -L/10 & 3/5 & 0 \\ 0 & -L^2/60 & 0 & L^2/10 \end{bmatrix}. \quad (10)$$

The complete stiffness matrix is the summation of the bending stiffness, initial constant tension stiffness, and the varying tension stiffness,

$$[k]_{TOT} = [k]_{EI} + [k]_{T_0} + [k]_{T'}. \quad (11)$$

Damping Matrix

Equivalent viscous damping is used as part of this analysis. Hydrodynamic damping is also used in this analysis, it arises only when relative motion is considered. The hydrodynamic damping will be further discussed with the wave force derivation. An equivalent

percentage of critical damping is input for the viscous damping to be used. The input allows different percentages of critical damping to be applied to any mode of vibration. The viscous damping can be formed through uncoupling the equations of motion by introducing modal transformations (Paz, 1980). This provides a diagonal matrix whereby each diagonal term represents a mode which can be assigned a percentage of critical damping,

$$[\Phi]^T [C]_M [\Phi] = 2\omega_{n_i} \beta_i \delta_{ij} = [A] . \quad (12)$$

The damping matrix can be calculated by

$$[C]_M = \left[\begin{array}{c} [\Phi]^{-1} \\ [A] [\Phi]^{-1} \end{array} \right]^T . \quad (13)$$

The advantage of orthogonality gives the following expression which is equivalent but computationally more efficient,

$$[C]_M = [M] \left[\begin{array}{c} N \\ \Sigma \\ i=1 \end{array} \right] 2\beta_i \omega_{n_i} \{\phi_i\} \{\phi_i\}^T [M] . \quad (14)$$

Eigen Analysis

The eigen analysis is performed in order to calculate the natural frequencies and mode shapes for the riser. They are needed for various reasons. One reason is that the aforementioned equivalent

viscous damping analysis makes use of the results. Secondly, if the natural frequencies fall within the expected zone of significant wave energy then a dynamic analysis would be warranted. The eigen analysis provides this needed information.

The undamped natural frequencies and mode shapes are solved using the characteristic equation (Bathe, 1982). A numerical procedure becomes essential for a 4 X 4 matrix or larger. Various iterative schemes are available for this purpose such as matrix deflation, the Jacobi method, and the Householder method. These procedures are well documented in many numerical analysis books, such as Bathe (1982). The generalized Jacobi method (Paz, 1980) is used in this thesis to obtain the natural frequencies and normalized mode shapes.

Current and Wave Forces

The current and wave forces are evaluated through the well known Morison's equation. Linearization of the non-linear drag term is accomplished by two methods. The first linearization method to be presented was first introduced by Borgman (1969a). The second linearization method was developed by Krolikowsky and Gay (1980).

The wave force equation can be written as

$$f = \frac{1}{2} \pi \rho C_m D^2 \dot{u}_w - \frac{1}{2} \pi \rho (C_m - 1) D^2 \ddot{y} + \frac{1}{2} \rho D C_d (u_w + u_c - \dot{y}) |u_w + u_c - \dot{y}| \quad (15)$$

The first term represents the inertial force due to the fluid acceleration around the riser. The second term represents a force

contribution which is a function of riser acceleration only, it is not dependent on the wave kinematics. Therefore, it is shifted to the left side of the equations of motion and is represented as an additional mass contribution; thus, the term added mass. The third term is the non-linear drag term which gives rise to the relative motion aspect of the riser problem. The non-linear drag requires the riser velocity value but the riser velocity is a result of the solved equations of motion, it is not known beforehand. This creates an iterative process for solving the equations of motion.

The wave kinematics are assumed as steady state harmonic motions. For solution convenience complex notation is used. The wave velocity is derived from linear wave theory as

$$u_w = u_0 e^{i\omega t}, \quad (16)$$

where

$$u_0 = \frac{Hkg \cosh kh}{2w \cosh kd} \quad (17)$$

and

$$e^{i\omega t} = \cos \omega t + i \sin \omega t. \quad (18)$$

It is understood that the real part of the solution is to be used.

Borgman Linearization Procedure

The drag force per unit length is given as

$$f_{\text{drag}} = \frac{1}{2} \rho DC_d (u_w + u_c - \dot{y}) |u_w + u_c - \dot{y}| . \quad (19)$$

The first assumption Borgman made in his linearization was that the mean value of the velocity was equal to zero; thus, the current effects would have to be handled separately from the wave effects. The results are linearly superimposed, a dynamic part and a static part,

$$f_{\text{drag}} = \frac{1}{2} \rho DC_d (u_w - \dot{y}) |u_w - \dot{y}| + \frac{1}{2} \rho DC_d u_c |u_c| . \quad (20)$$

Separating the two components introduces the major source of error with this method. Borgman's linearization method uses a least squares linear estimate equating the variance with the root mean square value. The result is

$$\frac{1}{2} \rho DC_d (u_w - \dot{y}) |u_w - \dot{y}| = \frac{1}{2} \rho DC_d \left[u_w - \dot{y} \right]_{\text{rms}} \left[8/\pi \right]^{\frac{1}{2}} (u_w - \dot{y}) . \quad (21)$$

Real notation becomes more convenient for the calculation of the root mean square value of the relative velocity,

$$\left[\left[u_w - \dot{y} \right]_{\text{rms}} \right]^2 = \frac{1}{2\pi/\omega} \int_0^{2\pi/\omega} \left[u_w - \dot{y} \right]^2 dt \quad (22)$$

where

$$u_w = u_0 \cos \omega t = \text{real part of } u_0 e^{i\omega t} \quad (23)$$

and

$$y = a \cos \omega t - b \sin \omega t = \text{real part of } (a+bi)e^{i\omega t} \quad (24)$$

with $a+bi$ representing the assumed complex form of the riser displacement. The result of the root mean square value is

$$\left[u_w - \dot{y} \right]_{\text{rms}} = \frac{1}{\sqrt{2}} \left[(u_0 + bw)^2 + (aw)^2 \right]^{\frac{1}{2}} . \quad (25)$$

The complete drag force becomes

$$f_{\text{drag}} = \frac{1}{2} \rho D C_d \left[\frac{8}{2\pi} \right]^{\frac{1}{2}} \left[(u_0 + bw)^2 + (aw)^2 \right]^{\frac{1}{2}} (u_w - \dot{y}) + \frac{1}{2} \rho D C_d u_c |u_c| . \quad (26)$$

Krolikowsky and Gay Linearization Procedure

This linearization method uses a Fourier series representation which allows proper inclusion of the current effects. Recalling the drag term, equation (19),

$$f_{\text{drag}} = \frac{1}{2} \rho D C_d (u_w + u_c - \dot{y}) |u_w + u_c - \dot{y}| . \quad (19)$$

The linearization method provides a drag term of final form

$$f_{\text{drag}} = \frac{1}{2} \rho D C_d B_1 (u_w - \dot{y}) + \frac{1}{2} \rho D C_d B_2 u_c , \quad (27)$$

where B_1 and B_2 are evaluated through the linearization method.

Again, real notation becomes more convenient. Equations (23) and (24) are combined to obtain

$$u_w - \dot{y} = (u_0 + bw) \cos \omega t + aw \sin \omega t , \quad (28)$$

which can be rewritten as

$$u_w - \dot{y} = A \sin(\omega t + \theta) \quad (29)$$

where

$$A = \left[(u_0 + bw)^2 + (aw)^2 \right]^{\frac{1}{2}} \quad (30)$$

and

$$\tan \theta = \frac{u_0 + bw}{aw} \quad (31)$$

Thus,

$$f_{\text{drag}} = \frac{1}{2} \rho D C_d \left[A \sin(\omega t + \theta) + u_c \right] \left| A \sin(\omega t + \theta) + u_c \right| \quad (32)$$

The Fourier series representation is written as

$$f_{\text{drag}} = C_0 + \sum_{n=1}^{\infty} C_n \cos n(\omega t + \theta) + \sum_{n=1}^{\infty} D_n \sin n(\omega t + \theta) \quad (33)$$

where

$$C_0 = \frac{w}{2\pi} \int_0^{2\pi/w} f_{\text{drag}} dt \quad (34a)$$

$$C_n = \frac{w}{\pi} \int_0^{2\pi/w} f_{\text{drag}} \cos n(\omega t + \theta) dt \quad (34b)$$

and

$$D_n = \frac{w}{\pi} \int_0^{2\pi/w} f_{\text{drag}} \sin n(\omega t + \theta) dt \quad (34c)$$

for $n \geq 1$. Only the first order term is used since higher harmonics are assumed to supply small contributions. The integrations give constants of:

$$\text{for } u_c \geq A; \quad C_0 = \frac{1}{2} pDC_d (\frac{1}{2} A^2 + u_c^2) , \quad (35a)$$

$$\text{for } u_c < A; \\ C_0 = \frac{1}{2} pDC_d \frac{A^2}{\pi} \left[\left[1 + 2(u_c/A)^2 \right] \sin^{-1}(u_c/A) + 3(u_c/A) \left[1 - (u_c/A)^2 \right]^{\frac{1}{2}} \right] , \quad (35b)$$

$$\text{for all } u_c; \quad C_1 = 0 , \quad (36)$$

$$\text{for } u_c \geq A; \quad D_1 = \frac{1}{2} pDC_d 2Au_c , \quad (37a)$$

$$\text{for } u_c < A; \\ D_1 = \frac{1}{2} pDC_d \frac{8A^2}{3\pi} \left[\left[1 + \frac{1}{2}(u_c/A)^2 \right] \left[1 - (u_c/A)^2 \right]^{\frac{1}{2}} + \frac{3}{2}(u_c/A) \sin^{-1}(u_c/A) \right] . \quad (37b)$$

After the constants are reinserted into the Fourier series representation the drag force term in final form becomes, from equation (27),

$$f_{\text{drag}} = \frac{1}{2} pDC_d B_1 (u_w - \dot{y}) + \frac{1}{2} pDC_d B_2 u_c \quad (27)$$

where for $u_c \geq A$;

$$B_1 = 2u_c , \quad (38a)$$

$$B_2 = (A^2/2u_c) + u_c , \quad (38b)$$

and for $u_c < A$;

$$B_1 = \frac{8A}{3\pi} \left[\left[1 + \frac{1}{2}(u_c/A)^2 \right] \left[1 - (u_c/A)^2 \right]^{\frac{1}{2}} + \frac{3}{2} (u_c/A) \sin^{-1}(u_c/A) \right], \quad (39a)$$

$$B_2 = \frac{A^2}{\pi u_c} \left[\left[1 + 2(u_c/A)^2 \right] \sin^{-1}(u_c/A) + 3(u_c/A) \left[1 - (u_c/A)^2 \right]^{\frac{1}{2}} \right]. \quad (39b)$$

After the linearization of the drag force is performed the drag term can be split into two contributions, a drag due to the water velocity and a drag due to the structure velocity. The drag due to the structure velocity is shifted to the left side of the equations as a hydrodynamic damping contribution. The relative motion assumption is the cause of the hydrodynamic damping contribution. For a riser analysis the relative motion and hydrodynamic damping are important assumptions. Without relative motion considerations the displacements and stresses are usually overpredicted.

Directional Seas

Knowledge of wave kinematics is essential to the proper wave force calculation upon a riser. Typical unidirectional waves tend to overpredict flow kinematics. Using a higher-order wave theory to better match the flow kinematics did not improve results much when compared to actual measurements. But, Forristall et al.(1978) used a linear wave theory combined with a directional spreading function to

match measured velocities and accelerations very closely. The flow kinematics matched better than when a high order unidirectional theory was used.

The directional spectrum is assumed to be separable and can be expressed as the product of a unidirectional wave energy spectrum and a directional spreading function,

$$E(w, \phi) = E(w)D(\phi) \quad . \quad (40)$$

Fig. 3 provides a good picture for the concept. The directional spreading function is designed to distribute but not alter the total wave energy content. Since the total energy content is not altered but only redistributed over direction then the following integral results,

$$E(w) = \int_{-\pi}^{\pi} E(w, \phi) d\phi \quad . \quad (41)$$

With this known an additional property of directional seas may be derived,

$$\int_{-\pi}^{\pi} D(\phi) d\phi = 1 \quad . \quad (42)$$

Various directional spreading functions have been proposed over time. The difficulty arises of describing an appropriate spreading function since the true directional spread of ocean waters is random

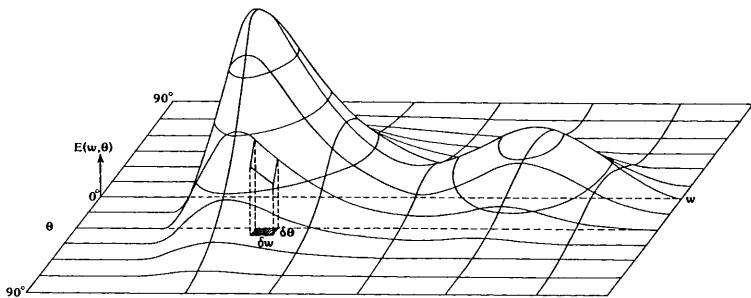


Fig. 3. Directional Energy Spectrum

and is based upon many different parameters. A cosine power spreading function is a popular choice for several reasons. The cosine power spreading function is rather straightforward and its few parameters are easily handled. The degree of directional spreading is easily accommodated with a specified concentration factor. The concentration factor can easily be specified to approximate a unidirectional spectrum as opposed to a directional spectrum. The cosine power spreading function has been shown to provide a good fit when compared to actual measurements. These reasons provide the impetus for choosing the cosine power spreading function from Forristall et al. (1978),

$$D(\bullet) = \frac{2^{2s-1} \Gamma^2(s+1)}{\pi \Gamma(2s+1)} \cos^{2s}[\frac{1}{2}(\bullet - \bar{\bullet})] , \quad (43)$$

where $D(\bullet)$ exists for $|\bullet - \bar{\bullet}| \leq \pi$. Borgman (1969b) presented an alternative spreading function,

$$D(\bullet) = \frac{2^{2s} \Gamma^2(s+1)}{\pi \Gamma(2s+1)} \cos^{2s}(\bullet - \bar{\bullet}) , \quad (44)$$

where $D(\bullet)$ exists only for $|\bullet - \bar{\bullet}| \leq \frac{1}{2}\pi$. Additionally,

$$\int_{-\frac{1}{2}\pi}^{\frac{1}{2}\pi} D(\bullet) d\bullet = 1 . \quad (45)$$

An additional simplification results when the concentration factor is an integer,

$$\Gamma(n) = (n-1)! \quad (46)$$

where n is any integer. The resulting expression for an integer valued concentration factor is

$$D(\bullet) = \frac{2^{2s} (s!)^2}{\pi (2s)!} \cos^{2s}(\bullet - \vec{\theta}) \quad (47)$$

The larger the concentration factor the more concentrated the spreading function becomes. Theoretically, as the concentration factor approaches infinity the directionally spread sea approaches the unidirectional sea.

The unidirectional energy spectrum chosen for this thesis is the Pierson-Moskowitz spectrum from Comstock(1967) which is of the form

$$E(w) = \frac{.0081g^2}{w^5} \exp \left[\frac{-.74g^4}{V^4 w^4} \right] \quad (48)$$

The Pierson-Moskowitz spectrum has been shown to adequately describe the wave energy as a function of wind velocity and wave frequency. The properties of the spectrum are available knowing the derivation of the energy spectrum. For this spectrum the significant wave height is related to the spectral area,

$$H_s = 4 [m_0]^{1/2} \quad (49)$$

where

$$m_0 = \int_0^{\infty} E(w) dw \quad . \quad (50)$$

Recall that the directional energy spectrum, $E(w, \phi)$, contains an equivalent amount of energy as the unidirectional energy spectrum, $E(w)$; thus, the spectral volume under the directional energy spectrum (see Fig. 3) is equivalent to the spectral area under the unidirectional energy spectrum. The resulting equivalent expression for m_0 is

$$m_0 = \int_0^{\infty} \int_{-\frac{1}{2}\pi}^{\frac{1}{2}\pi} E(w, \phi) d\phi dw \quad . \quad (51)$$

Responses and Numerical Procedures

Basic Procedure

The addition of the mass, damping, and stiffness element matrices provides the global constraining matrix equations of motion. The nodal forces and corresponding global force array are calculated through integration of the wave and current forces per unit length. Numerical integration is used due to the complexity of integrating the force per unit length exactly. While the commonly used Simpson's rule is an adequate method, more efficient methods of numerical integration

exist. Numerical quadrature techniques, as described in Bathe(1982), are used. Ten-point Gaussian quadrature is the technique used and it is capable of integrating up to a nineteenth order polynomial exactly; thus, only ten points are required for integration of the force along a specified element. The final matrix equations of motion are

$$[M]\{\ddot{y}\} + [C]\{\dot{y}\} + [K]\{y\} = \{F\} \quad (52)$$

where

$$[C] = [C]_M + [C]_H . \quad (53)$$

The steady state harmonic displacements of the riser are assumed of the complex form

$$y = y_0 e^{i\omega t} . \quad (54)$$

Using this complex notation along with the complex notation of the water particle velocity provides an $e^{i\omega t}$ term on both sides of the equations of motion. The term can be cancelled from both sides thus eliminating the time component. The complex nodal displacements are solved for in this manner.

The time-invariant displacement can be solved for separately from the time-dependent displacement. Superposition of both displacements provides the total displacement.

The static displacement is the displacement due to the current effects and the proposed static offset. It depends upon the stiffness matrix only and does not include inertial or damping effects. The top node of the riser is assumed to have a static offset equal to an input

percentage of the water depth. The penalty method(Bathe, 1982) is used to constrict the top node of the riser to the specified offset. The current force effects are accounted for simultaneously. The penalty method provides an error contribution since the current force on the top node of the riser is essentially negated through the penalty method formulation. The consequences of this error are minor when one considers that vessel motion is the dominating contribution for riser motion at its top end. The static displacement is calculated through this method.

The time-dependent motion of the riser is solved while accounting for the time-varying forces and inertial, damping, and stiffness effects. Vessel motion at the riser's top end is accounted for through the used of response amplitude operators with appropriate phasing at a specified wave period. These input data are available from ship motion programs and the methods for obtaining them are not discussed here. As with the static case, the penalty method is used to constrict the riser top end motion to the vessel motion; thus, the wave force contribution at the top end of the riser is negated. The inclusion of damping effects provides a complex matrix since a component ninety degrees out of phase is included. Inverting this complex matrix(which accounts for the mass, damping, and stiffness) and multiplication with complex forces provides the complex displacements. The process described here is an iterative process since the hydrodynamic damping and the wave force are dependent upon the riser velocity. Convergence within a specified limit is usually

reached in three to ten iterations.

The complex dynamic displacement is linearly superimposed to the static displacement to find the total displacement. For each case involving a static offset there will be a maximum displacement and a minimum displacement. Once the displacements are known then bending stresses can be calculated.

Bending stresses within a riser can be calculated through various methods. The most common method uses the stress-strain matrix, a result of finite element analysis, in order to calculate the stresses. The stress-strain matrix requires the resulting deflections and rotations. In the analysis used for this thesis, condensation is used to reduce the total number of degrees of freedom. The problem results in rotational degrees of freedom being condensed out; thus, calculation of the stresses from the stress-strain matrix is not possible. Another method, one which is used in this thesis, makes use of geometrical considerations in order to obtain the stresses.

The method, presented by Morgan(1975), calculates the radius of curvature along the riser from which the bending stress is calculated. Once the radius of curvature is known then the moment is calculated from

$$M = \frac{EI}{R} \quad (55)$$

Finally, the stress is found from

$$\sigma = \frac{M\bar{y}}{I} . \quad (56)$$

The method assumes that no element stretching exists. Bending stresses are calculated along the riser from this method. The maximum bending stresses are recorded along the riser length giving rise to an envelope. This is accomplished by passing the steady state wave by the riser and continuously calculating the bending stresses as the wave passes.

Directional Response Considerations

In order to calculate responses in irregular seas a few assumptions must be made. The first is that an irregular sea can be considered as being a summation of many small amplitude regular waves. Secondly, the sum of the responses to these regular waves is equal to the response due to the sum of the waves. A third assumption is that the response at each wave period is linearly proportional to the wave height. Model tests have confirmed these assumptions (Minkenberg and Gie, 1974) for vessels in small amplitude waves and it is possible to extend these assumptions to include a riser.

The first step in applying the foregoing assumptions into calculating responses is to discretize the spectrum into a number of regular waves. The basic procedure is well outlined (Comstock, 1967) for a vessel response calculation. The directional spectrum is discretized into an adequate number of frequencies and directions.

Using more discretizations will give better results although using too many may become costly. The wave height for each discretized volume is calculated by

$$H = 2 \left[2E(w_j, \phi_j) \delta w \delta \phi \right]^{\frac{1}{2}} \quad (57)$$

where δw and $\delta \phi$ are differential increments of frequency and direction. Fig. 3 shows a discretized volume of the directional spectrum. Knowledge of the wave height, wave period, and vessel response amplitude operator for the specific period and direction provides the needed information to obtain a unidirectional, planar riser response. Once the riser response is calculated a transfer function can be obtained for the vessel/riser system versus wave height,

$$TF(w_j, \phi_j) = \frac{2y_0}{H} \quad (58)$$

The transfer function is of the form of a riser peak-to-peak response divided by the wave height. The assumption of linear response with wave height must be maintained, though, and this presented a problem.

The drag force term in Morison's equation provides a squared wave height term. The linearization methods incorporated in this thesis do not provide a linear response with wave height but other linearization methods are available which do. This problem had to be addressed. Before changing linearization methods to account for a linear wave height much thought was given to the effects of eliminating drag altogether. As was mentioned earlier, riser response to directional

seas is considered to have a large impact for low energy seas, not for high energy design waves. With small wave heights the wave force becomes inertially dominated; thus, the drag can be neglected.

Marshall(1976) observed for wave height-to-diameter ratios less than 4 that neglecting the drag force term altogether will result in errors less than 5%. This provides a firm basis for neglecting the drag for the small waves typical in low energy seas. Should the wave heights increase and drag forces begin to dominate then the drag force would have to be linearized by other methods incorporating a linear wave height term.

By neglecting the drag force the relative motion consideration is lost. This is an undesirable result since the hydrodynamic damping contribution is very significant for waves near the riser natural frequencies. Without the inclusion of some type of damping the results could be useless. Thus, account had to be made of damping. As was mentioned earlier, the ability to use an equivalent viscous damping is available. This solves the problem of accounting for the hydrodynamic damping which is unavailable without relative motion. Now another problem arises as to what the percentage of critical damping should be. By comparing computer runs with and without hydrodynamic damping the equivalent percentage of critical damping was evaluated. Typical values of 15% to 20% of critical damping were observed. It was recognized that these values are sensitive to wave height and period. The commonly used values of 3% - 5% were for fixed installations where the effects of relative motion are usually small.

But, the riser is a dynamically oscillating structure with large displacements and velocities so the high percentages of critical damping are not unexpected.

Once the transfer function of the vessel/riser system is known for each period and direction then the directional displacement spectrum can be obtained. The volume under the directional displacement spectrum is then used to provide statistical displacements. The volume is

$$S_x = \int_0^{\infty} \int_{-\frac{1}{2}\pi}^{\frac{1}{2}\pi} \left| \text{TF}(w_j, \phi_j) \right|^2 E(w_j, \phi_j) d\phi dw \quad (59)$$

where

$$\left| \text{TF}(w_j, \phi_j) \right| = \text{the modulus of } \text{TF}(w_j, \phi_j) .$$

The integration is performed by using Simpson's one-third rule. The significant displacement is then available using the appropriate Rayleigh constant for the Pierson-Moskowitz spectrum used. The significant displacement represents the peak-to-peak displacement,

$$R_{\text{sig}} = 4 (S_x)^{\frac{1}{2}} . \quad (60)$$

Once the significant displacement for each node is known then the stresses can be determined. A problem arises in the frequency domain in that all phasing information is lost. Only the magnitudes of the displacements are known. This thesis assumes that the significant displacements occur at the same time. Although the assumption is not

necessarily correct it does represent a fairly good approximation. The stresses are based upon the significant nodal displacements and are calculated by the same method as for the unidirectional, planar riser cases.

III. NUMERICAL RESULTS

Comparison With API Codes

The riser model used for this study was based on a unidirectional wave model described in an American Petroleum Institute(API from here on) bulletin on marine risers(API, 1977). The bulletin's function was to compare eight industrial riser programs. Results from the submitted cases varied but an overall pattern was produced. The API bulletin now provides a basis from which other marine riser programs can be compared. Comparison with the API codes is used in order to verify the riser computer program written for this thesis.

Two cases were used to verify the riser model, one at 500 feet of water depth and one at 1500 feet of water depth. The API data for the cases is presented in Table 2. The displacements and bending stresses for each case are compared with the API results.

The displacements and bending stresses for the 500-foot water depth are shown in Figs. 4 and 5. The displacement curves represent the minimum and maximum excursions of the riser during its steady state response. For example, for the riser top end, the static offset is 15 feet with a dynamic displacement of ± 2 feet; thus, a 13-foot minimum displacement and a 17-foot maximum displacement. The bending stress curve represents the maximum bending stress at each node during the riser steady state response. The maximum stresses don't

Table 2. Riser Properties

500 ft and 1500 ft Water Depths

Riser Outside Diameter	16.00 in
Riser Inside Diameter	14.75 in
Riser Modulus of Elasticity	30 X 10 ⁶ psi
Drilling Mud	89.8 lb/ft ³
Weight in Air of 50' Pipe Joint	8621 lb
Sea Water Specific Weight	64 lb/ft ³
SWL to Riser Support Ring	50.0 ft
Seafloor to Lower Ball Joint	30.0 ft
Drag Coefficient	0.7
Inertia Coefficient	1.5
Effective Diameter for Wave Force	26.0 in
Static Offset(% of Water Depth)	3.0%
Current:	½ knot at SWL, zero at lower ball joint
Wave Height	20.0 ft
Wave Period	9.0 secs
Vessel Surge Amplitude(Peak to Peak)	4.0 ft
Vessel Surge Phase Angle(Vessel Lags Wave Crest)	15°

	<u>500 ft Water Depth</u>	<u>1500 ft Water Depth</u>
Riser Length	520 ft	1520 ft
Top Tension	120 kips	290 kips

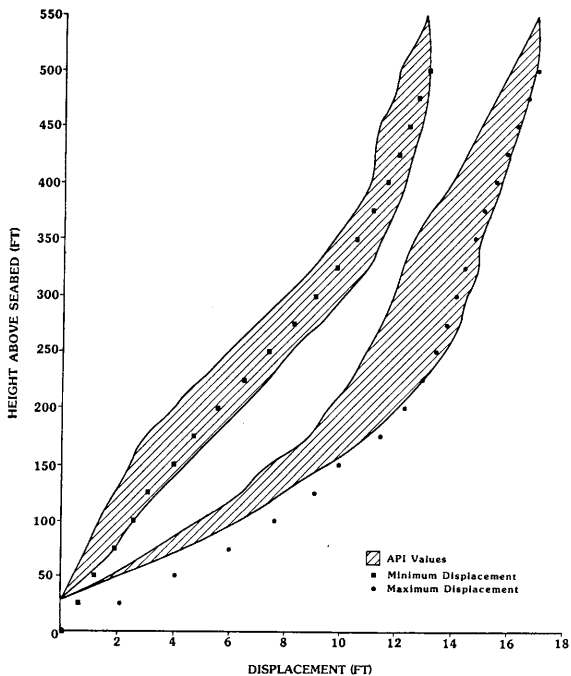


Fig. 4. Displacement Ranges for API Comparison- 500 ft Depth

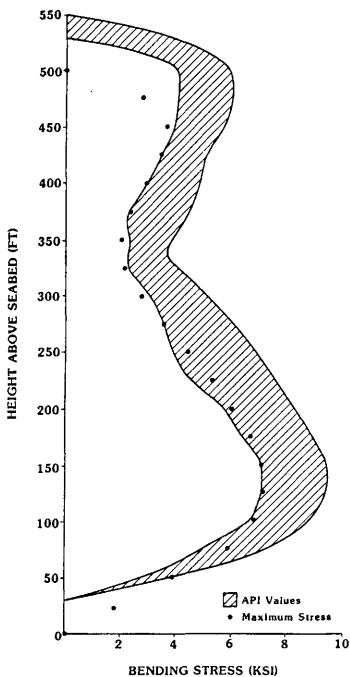


Fig. 5. Maximum Bending Stresses for API Comparison-
500 ft Depth

necessarily occur at the same time, though. This provides an envelope of expected maximum bending stresses. Results of the 500-foot water depth compare well except for near the top of the riser. This is due to the assumed boundary condition locations along the riser. For this riser study it was assumed that the riser would be pinned at the seafloor and would extend to the still water level only, a riser length of 500 feet. The riser cases submitted for the API study assumed the riser to be pinned at the lower balljoint, 30 feet above the seafloor, with an extension to the slip ring, 50 feet above the still water level, a length of 520 feet. The minor disparity in the results near the riser top are accounted by this reason. The assumption is not a poor one for a few reasons. The first is that the results still agree well throughout the remaining riser length. Secondly, the maximum bending stresses are the most important values needed from a riser analysis and the maximums occur near the bottom for the majority of dynamic riser analyses. Results compare very well near the bottom so the maximum values are preserved. Thirdly, and maybe the most important reason, the essence of the thesis involves comparisons and as long as the riser model is consistent then the comparisons won't be affected. Note that the disparity of bending stress near the riser top end is not as great for the 1500-foot water depth case, Figs. 6 and 7. This is as expected since a 30-foot difference in the blow-out-preventer to seafloor clearance is a smaller error for a 1500-foot water depth than for a 500-foot water depth. Note that results compare very well for the 1500-foot case as

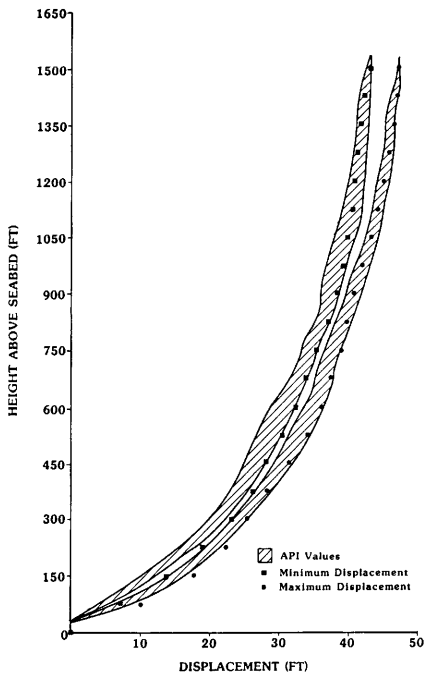


Fig. 6. Displacement Ranges for API Comparison-
1500 ft Depth

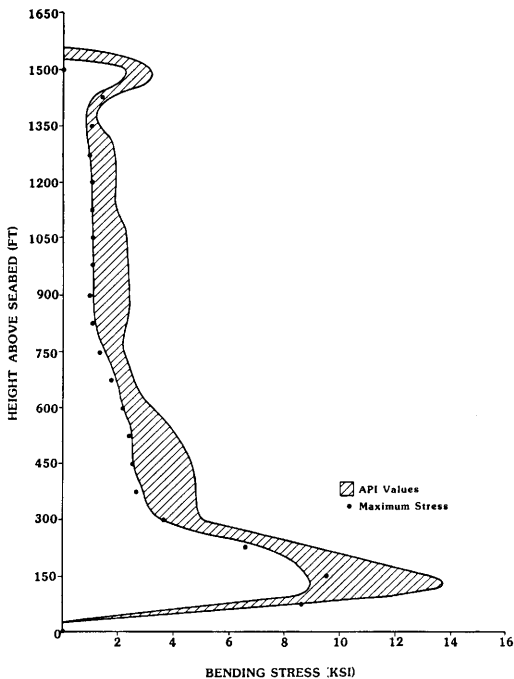


Fig. 7. Maximum Bending Stresses for API Comparison-
1500 ft Depth

with the 500-foot case. Based upon the two comparison cases it is evident that an acceptable riser model has been developed.

It should be reiterated that in this study the stress distribution along the riser is evaluated using only the nodal displacements. The procedure used is accurate in regions where the curvature is discernable. However, in situations where two consecutive finite elements are nearly parallel the evaluation of the radius of curvature is quite sensitive and very susceptible to error. This was observed in the stress calculation near the ball joint connected to the lower marine riser package. Since this is a localized numerical problem, it in no way affects the stress evaluation in the critical regions. However, the numerical values in the region where this occurred were adjusted to reflect the expected values.

For the remainder of the results the 500-foot water depth case is to be used. This is primarily because many existing vessel/riser systems are currently being utilized in water depths of approximately 500 feet.

Vessel Phasing Comparison Cases

Of particular importance to many frequency domain riser analyses is the topic of vessel phasing with respect to the wave. Some riser analyses, especially stochastic analyses, ignore or are unable to account for vessel phasing with respect to the wave. Three test cases

are examined in order to account for the effect of vessel phasing. The three cases are for a vessel lagging the wave crest by 90° , a vessel lagging the wave crest by 45° , and a vessel in phase with the wave crest, 0° . The resulting displacements and stresses for the three cases are compared in Figs. 8 and 9. It is evident that a wide disparity is present between the three cases. The bending stresses located 125 feet from the seafloor vary widely with the 0° vessel phase value being more than twice the value of the 90° vessel lag value. In this sense it is observed that phasing is important. But, for the riser analyses which don't account for the phasing the maximum values are preserved. Cases in which the vessel led the wave crest by 45° and 90° were examined but were not presented since they closely resembled the 0° phasing case. Although slightly larger values were observed, the differences in response over the 0° phasing case were very small, not nearly as pronounced as the response differences between the 0° phase and lagging cases. This is a result of the increased hydrodynamic damping due to the larger wave forces for the vessel lead cases. Thus, the assumption of using no phasing will not necessarily provide the true results but will almost always provide the worst cases to be encountered. When performing a fatigue analysis vessel phasing would be of importance since low stress, high cycle runs are performed. Accurate displacements and stresses are required in those instances, not the expected maximum values. If the desired results are the maximum values then using 0° vessel phasing will provide them.

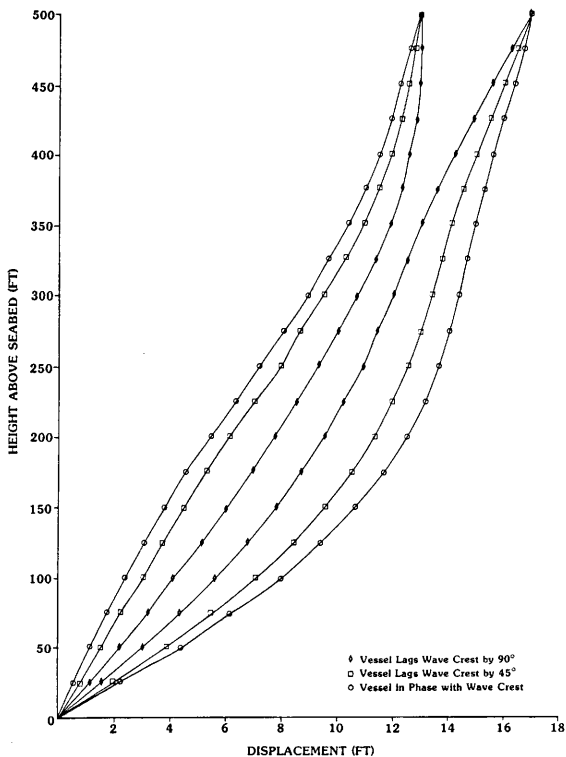


Fig. 8. Displacement Ranges for Vessel Phasing Comparison

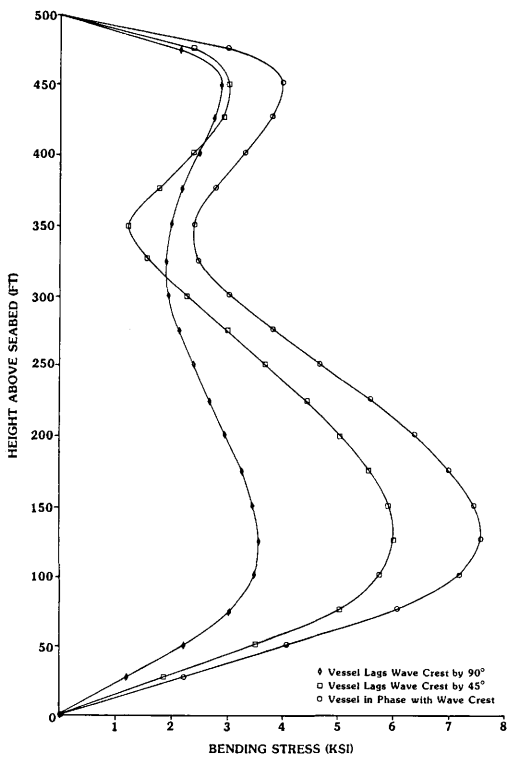


Fig. 9. Maximum Bending Stresses for Vessel Phasing Comparison

Linearization Method Comparison Cases

As previously discussed, when using a solution in the frequency domain the drag force requires linearization. The objective of the linearization is to fit the actual non-linear form of the drag force as closely as possible. Borgman's(1969a) method is compared against the newer, more accurate, method proposed by Krolikowsky and Gay(1980). The essential difference between the two methods is that with Borgman's analysis the current must be accounted for separately from the wave while Krolikowsky's analysis allows for direct wave-current coupling interaction. Since the actual environment exhibits wave-current interaction effects Krolikowsky's method seems more reasonable. He demonstrated this to be true while comparing his technique and Borgman's technique against the actual non-linear form of the drag force. Krolikowsky made some sensitivity analyses exploring critical regions where each method converged or diverged around the actual non-linear drag force form. The sensitivity parameter was u_c/A . Recalling equation (30),

$$A = \left[(u_0 + bw)^2 + (aw)^2 \right]^{\frac{1}{2}}, \quad (30)$$

where $a+bi$ is the structural displacement. A value of $u_c/A = 1$ provided the point at which the Krolikowsky method converged closely to the actual non-linear form while the Borgman method diverged heavily.

Figs. 10 and 11 present the results of comparing the two linearization methods. Three cases of u_c/A were examined; $= \frac{1}{2}$, $= 1$, and $= 2$. Borgman's method is seen to underpredict the displacements and stresses when compared with Krolikowsky's method. This is an expected result since the force from Borgman's method is generally smaller. It is noticed that the stresses near the riser bottom are almost identical for both cases. This may indicate that bottom stresses may be mostly due to other factors besides wave and current forces, such as the specified offset and vessel motion. Thus, bottom stresses are similar for each method. Near the riser top end is where wide disparities result. It is evident that stresses near the riser top are controlled to a large part by wave and current forces since the stresses differ significantly for each method. The linearization method of Krolikowsky's provides the greater stresses; thus, if stresses near the riser top are of importance then the Krolikowsky linearization method is a must. Probably the most important conclusion regarding the results lies with the ascertainment of the maximum expected stress. For most riser analyses the maximum bending stress occurs near the bottom of the riser. Using the linearization method of Krolikowsky's tends to increase the top end stresses. The top end stresses may increase enough to become the maximum stresses occurring in the riser. This can be of great importance to the overall design. With Borgman's method providing smaller top end stresses the maximum stress may be unaccounted for. Thus, concern is warranted when top end stresses begin to approach maximum stress

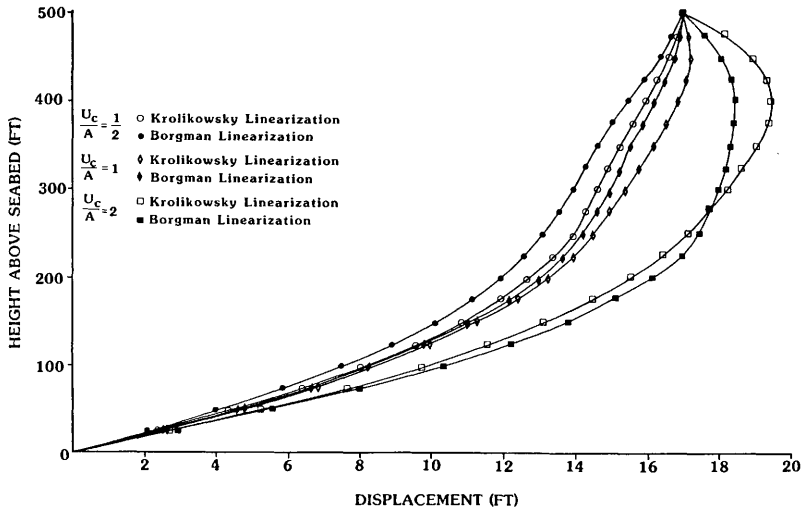


Fig. 10. Maximum Displacements for Linearization Comparison

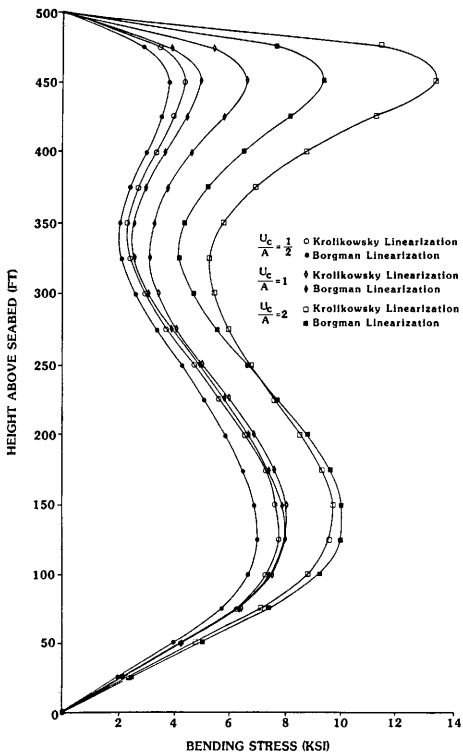


Fig. 11. Maximum Bending Stresses for Linearization Comparison

values usually located near the riser bottom. With the use of Krolikowsky's linearization method the top end stresses may exceed the bottom stresses in the riser.

Directional Sea Responses

The directional sea responses are based upon essentially the same riser data as presented in Table 2. However, a few differences exist which warrant discussion.

When calculating directional riser responses some three-dimensional aspects are included. The question arises as to the form of the ocean currents. Three-dimensional currents exist but difficulties arise when trying to quantify them. Also, resolving a given three-dimensional current into various directional planes might contribute significant errors since procedural uncertainties exist. Better knowledge of three-dimensional currents is needed before accurate planar configurations can be determined. Due to the uncertainties regarding three-dimensional currents it was decided to neglect all current effects. Once accurate data is available then further research on the effects can be performed.

Similar arguments exist for the proposed static offset. Inclusion of a static offset in a specified plane is difficult to define from a three-dimensional viewpoint. No static offset was used for the directional response cases.

For the steady state unidirectional waves a significant wave

height and period were specified as inputs. These quantities are now a function of the Pierson-Moskowitz wave energy spectrum. The wind speed measured 64 feet above the still water level is the input used to describe the spectrum. The spectral shape is then used to determine the significant wave height and period. Wind speeds of 20 knots and 40 knots are used for the sensitivity cases. The 20-knot wind would supply a low energy sea while the 40-knot wind would supply a storm sea. A 20-knot wind would have a significant wave height of 7.4 feet and a period of 5.3 seconds. A 40-knot wind would have a significant wave height of 29.6 feet and a period of 10.7 seconds.

The most significant factor affecting the directional riser response is the vessel motion. Two different types of vessels are compared for the directional cases, a cylindrical platform and a drillship. Response amplitude operators (RAO) for the vessels are given in Fig. 12. The surge case represents the maximum response direction and the vessels are symmetric around that direction. The RAO values located $\pm 45^\circ$ around the surge direction are supplied. Information was unavailable regarding the $\pm 90^\circ$ RAO values. In response to this the $\pm 90^\circ$ RAO values were assumed to be identical to the $\pm 45^\circ$ RAO values. Vessel phasing information with respect to the wave crest was also unavailable so values of 0° phase were used. The surge direction was assumed to be the wave mean peak energy direction since this represents the worst-case direction. RAO values between the given 0° and $\pm 45^\circ$ curves were obtained using linear interpolation.

In response to the neglected drag force the drag coefficient had

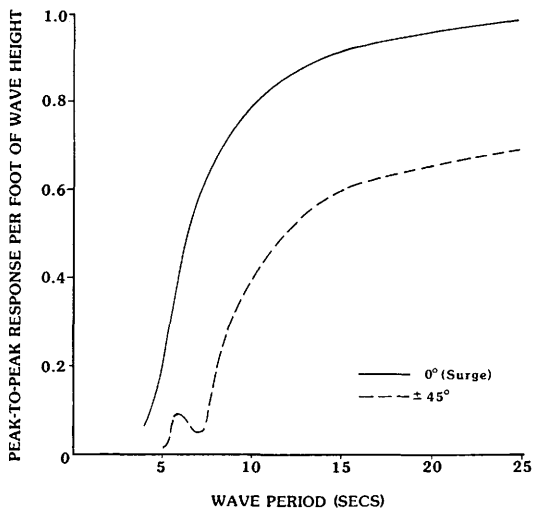


Fig. 12. Vessel Response Amplitude Operators

to be set equal to zero. This nullifies all drag force and relative motion considerations. As a consequence to this all cases with significant drag force effects must be carefully scrutinized. Since the relative motion aspect is also negated careful consideration must be given to the percentage of critical damping which is an input. This damping is intended to supply an equivalent viscous damping accounting for the loss of hydrodynamic damping. The damping contribution is important and it must be used to correctly account for the loss of hydrodynamic damping ordinarily available through relative motion. A value of 15% of critical is used for the test cases. In actuality, the percentage of critical damping is dependent upon many different parameters such as wave height and period.

The degree of wave spreading is determined by the specified concentration factor. Three distinct wave spreading cases were examined in these test cases. Concentration factors of 1, 3, and 25 were chosen based upon correlation with available gulf of Mexico data. Factors equal to 1 and 3 represent directionally-spread seas while a factor of 25 essentially represents a unidirectional wave. Fig. 13 shows the variation in angular spread of each.

The first sensitivity analysis involves a comparison between a cylindrical platform and a drillship. The cylindrical platform has similar RAO values in all directions while the drillship has varying RAO values over direction. The cylindrical platform RAO values are from the surge curve in Fig. 12 while the drillship uses the RAO values interpolated around the surge curve. The wave mean peak

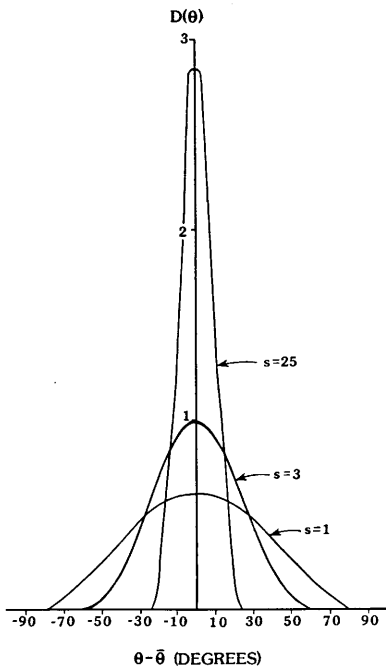


Fig. 13. Comparison of Spreading Concentration Factors

direction was assumed to act in the surge direction, the worst-case direction for each vessel. Figs. 14, 15, 16, and 17 show the displacements and stresses for the 20-knot and 40-knot cases. The directional sea displacement figures represent one-half of the peak-to-peak displacement. The cylindrical platform displacements and stresses are higher than those of the drillship. This is as expected since the surge RAO values represent the worst-case direction and the cylindrical platform has these worst-case RAO values in all directions. RAO values for the drillship are smaller away from the surge direction. Had the wave mean peak direction been chosen as another direction, such as sway, then the trends would not have been the same. But, design and fatigue analyses are tested on a worst-case direction so justification exists for choosing the wave mean peak direction equal to the worst-case direction. Note that the results for the drillship depend upon the degree of spread of the waves. This is not the case for the cylindrical platform, though. Since the cylindrical platform has similar RAO values in all directions then altering the spread of the waves will not alter the significant responses. Recall that the spreading function merely redistributes energy over direction, it does not alter the total energy content. Thus, similar results would be obtained using any spreading concentration factor for the cylindrical platform case. Conclusively, the drillship has smaller displacements and stresses than the cylindrical platform for the wave mean peak direction aligned with the worst-case RAO values.

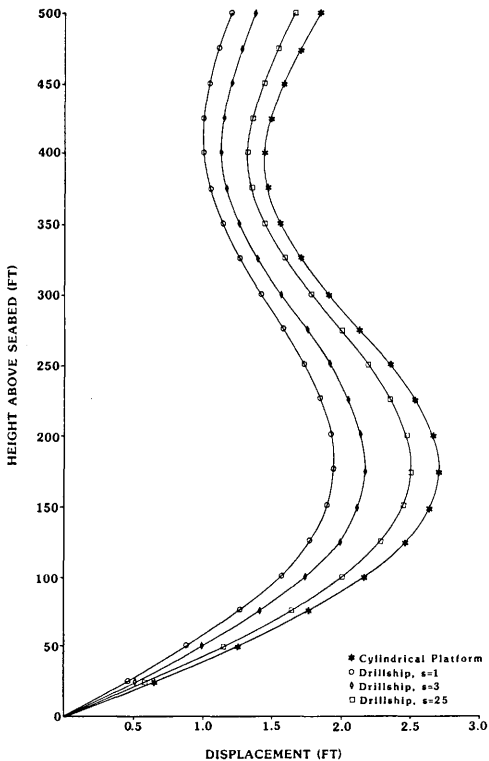


Fig. 14. Displacements for Directional Seas- 20 Knots

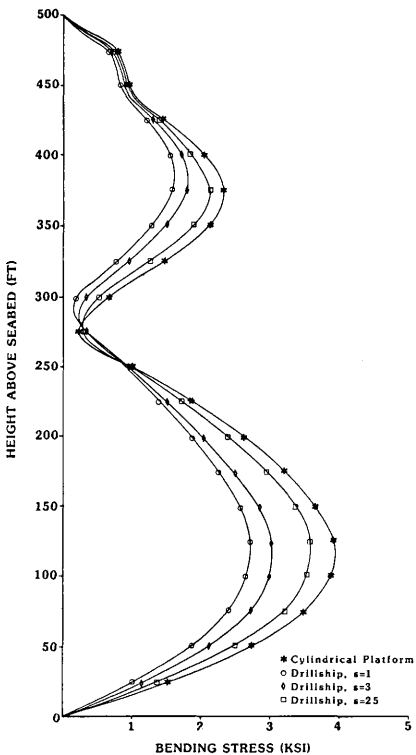


Fig. 15. Bending Stresses for Directional Seas- 20 Knots

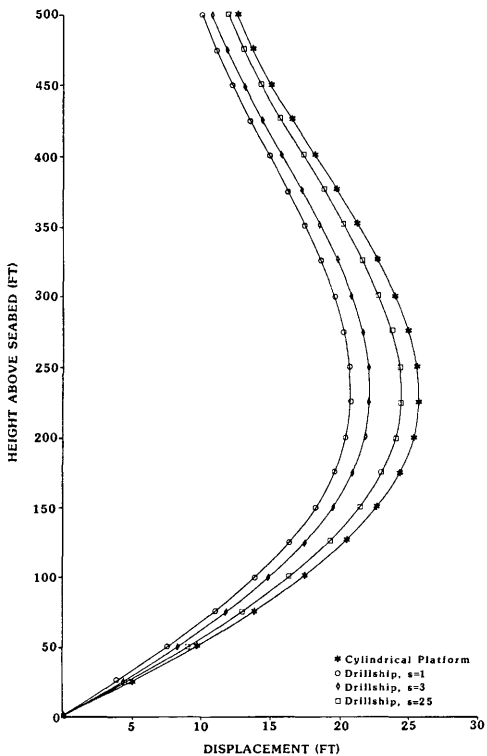


Fig. 16. Displacements for Directional Seas- 40 Knots

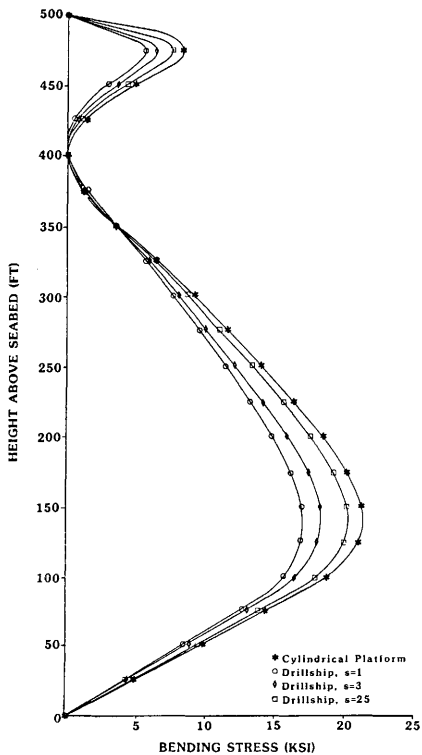


Fig. 17. Bending Stresses for Directional Seas- 40 Knots

The second sensitivity analysis involves a comparison between the degree of wave spreading. Figs. 14, 15, 16, and 17 also show the results of these cases. The results do vary for the effects of wave spread on the drillship. The responses for a largely spread sea are smaller than for a concentrated sea. This is as expected since the drillship RAO values decrease away from the surge direction, also the wave mean peak direction. Integration of these smaller response energies provides a smaller total response. For the case of a concentrated sea the wave tends to act as a unidirectional sea. Since the drillship RAO values are larger towards the mean peak direction of the unidirectional wave then the total responses will be larger. This is reflected in the results. As the concentration factor increases then the directional sea approaches the unidirectional sea. Should the worst-case drillship RAO values exist along the mean peak direction of the wave then the worst-case results are expected. Note that all these results are dependent upon the largest drillship RAO values being aligned along the mean peak direction of the sea.

The responses for the 40-knot wind case appear reasonable but they deserve additional discussion. Recall that the drag force and hydrodynamic damping effects are neglected. This could be a source of significant error for the 40-knot wind case where drag effects may be important. The loss of the drag force contribution is important but it is felt that the loss of the hydrodynamic damping may be the key consideration. For forcing frequencies near the vessel/riser natural frequencies inadequate damping can be a detrimental factor. Without

sufficient damping the results could be misleading and worthless. The importance of choosing an appropriate equivalent viscous damping percentage is stressed. For dynamic problems dealing with large displacements and large velocities the equivalent viscous damping percentage can be as high as 30% and even beyond.

Another interesting note to be discussed involves the 20-knot wind case. The displacements near the top end decrease before increasing, an extra inflection point. An extra inflection point also occurs in the bending stress curve as a result of this. This may be explained as a resulting vibration of the second mode. The deflected shape of the displacement curve resembles the second mode eigenvector shape. It was noted that the vessel/riser system's second natural frequency approximated the significant period of the 20-knot energy spectrum, thus, the excitation of the second mode. Since no appreciable wave energy was located near the first natural frequency of the system this mode of vibration was not excited. This is an important consideration to keep in mind when low energy seas are being considered as the primary type of wave excitation. An adequate number of lower modes must be included.

IV. SUMMARY AND CONCLUSIONS

This thesis investigated riser response to directional seas. Unidirectional model verification was achieved through a comparison with API codes. Effects of vessel phasing and drag force linearization methods were studied. Results dealing with different vessels and the effects of directional spreading were obtained.

The planar model was verified with the API codes for a unidirectional wave. Displacements and stresses for two cases, water depths of 500 ft and 1500 ft, were compared with published API results. The results compared favorably with the exception of minor disparities due to the assumed boundary condition locations.

The effects of vessel phasing on riser responses were studied. Displacements and stresses varied for the three cases. A 90° vessel lag provided the smallest response while a 0° vessel lag provided the largest response. Responses for the vessel leading the wave crest approximated the 0° results. If accurate responses are desired then the vessel phasing effects are important. If the maximum expected values are desired then vessel phasing can be neglected since a 0° phase provides the worst case results. Based on this investigation it is apparent that vessel phasing characteristics are a significant factor for design considerations.

Two drag force linearization methods were compared in order to ascertain the effects of each. Borgman's(1969a) technique represents

the original method while the Krolikowsky and Gay(1980) technique represents the updated method. Top end responses differ for the two techniques with the larger responses provided by the Krolikowsky and Gay(1980) method. Bottom responses in the riser are similar for both techniques. This would lead to the conclusion that bottom responses are affected more by offset and vessel motion as opposed to wave forces. The wave forces are noticed to play an important role in the top end responses, though. If the top end responses become significant then the more reasonable technique from Krolikowsky and Gay(1980) is recommended.

The directional responses were obtained using a Pierson-Moskowitz wave energy spectrum in conjunction with a cosine power spreading function. Responses were obtained for two cases, a 20-knot wind and a 40-knot wind. The wave mean peak direction was aligned with the worst-case vessel response direction. Note that the results are based upon this orientation and any other orientation would provide different results.

Cylindrical platform responses were compared with drillship responses. The drillship responses were smaller than the cylindrical platform responses. The reason for this is that the cylindrical platform had the worst-case RAO values in all directions while the RAO values for the drillship decreased away from the wave mean peak direction.

The effect of directional spreading showed that smaller responses were obtained for larger amounts of directional spread. This is a

result of the drillship RAO values decreasing away from the wave mean peak direction.

An interesting result appeared for the 20-knot wind case. Double inflection points occurred in the response curves indicating an excitation of the second mode of vibration. This is logical since the significant period of the 20-knot spectrum closely approximated the second natural frequency of the vessel/riser system.

The drag effects for the directional responses were neglected in order to satisfy the requirements of linear spectral techniques. The drag force contribution was lost altogether and the hydrodynamic damping contribution was accounted for through the use of an equivalent viscous damping. Small wave height, inertially dominated forces are able to satisfactorily circumvent this assumption as long as an appropriate equivalent viscous damping percentage is used. This is portrayed through the 20-knot wind case. Results from cases with significant drag effects deserve careful judgement as to the validity of the results. This is portrayed through the 40-knot wind case. Difficulty arose when deciding on an appropriate equivalent percentage of critical damping since the percentage of critical is dependent upon many parameters such as wave height and period.

Uncertainties exist as to the directional configurations due to three-dimensional currents and offsets. For these reasons both current and offset effects were neglected in the directional response calculations. With adequate knowledge of three-dimensional currents and offsets their inclusion in directional responses is possible.

The area of fatigue has the most to benefit from directional sea representations. Fatigue lives are traditionally based upon unidirectional seas in a worst-case response direction. Accounting for the large directional spread in the low energy seas could substantially increase fatigue lives.

REFERENCES

- API. 1977. API bulletin on comparison of marine drilling riser analyses. API BUL 2J, First Edition, American Petroleum Institute, Dallas, Texas.
- BATHE, K.J. 1982. Finite Element Procedures in Engineering Analysis. Prentice Hall, Englewood Cliffs, New Jersey.
- BERGE, B. and PENZIEN, J. 1974. Three-dimensional stochastic response of offshore towers to wave forces. Offshore Technology Conference paper 2050, 173-190, Houston.
- BORGMAN, L.E. 1969a. Ocean wave simulation for engineering design. Journal of Waterways and Harbors Division, ASCE vol. 95, No. WW4, 557-583.
- BORGMAN, L.E. 1969b. Directional spectra models for design use. Offshore Technology Conference paper 1069, 721-746, Houston.
- CHAKRABARTI, S.K. and FRAMPTON, R.E. 1982. Review of riser analysis techniques. Journal of Applied Ocean Research, vol. 4, No. 2, 73-90.
- COMSTOCK, J.P. 1967. Editor of Principles of Naval Architecture. SNAME, New York, New York.
- FORRISTALL, G.Z., CARDONE, V.J. and BORGMAN, L.E. 1978. The directional spectra and kinematics of surface gravity waves in tropical storm delia. Journal of Physical Oceanography, vol. 8, 888-909.
- GARDNER, T.N. and KOTCH, M.A. 1976. Dynamic analysis of risers and caissons by the element method. Offshore Technology Conference paper 2651, 405-420, Houston.
- GNONE, E., SIGNORELLI, P., and GIULIANO, V. 1975. Three-dimensional static and dynamic analysis of deep-water sealines and risers. Offshore Technology Conference paper 2326, 799-812, Houston.
- KROLIKOWSKY, L.P. and GAY, I.A. 1980. An improved linearization technique for frequency domain riser analysis. Offshore Technology Conference paper 3777, 341-353, Houston.
- MARSHALL, P.W. 1976. Dynamic and fatigue analysis using directional spectra. Offshore Technology Conference paper 2537, 143-157, Houston.

- MINKENBERG, H.L. and GIE, T.S. 1974. Will the regular wave concept yield meaningful motion predictions for offshore structures? Offshore Technology Conference paper 2040, 61-76, Houston.
- MORGAN, G.W. 1975. Dynamic analysis of deep water risers in three dimensions. ASME paper No. 75-PET-20.
- PAULLING, J.R. 1979. Frequency-domain analysis of OTEC CW pipe and platform dynamics. Offshore Technology Conference paper 3543, 1641-1651, Houston.
- PAZ, M. 1980. Structural Dynamics, Theory and Computation. Van Nostrand Reinhold Company, New York, New York.

APPENDIX. NOMENCLATURE

a	=	real part of complex displacement y_0
A	=	modulus of the water/riser relative motion
[A]	=	$[\phi]^T [C]_M [\phi]$
b	=	imaginary part of complex displacement y_0
B_1	=	drag force linearization coefficient
B_2	=	drag force linearization coefficient
C_0	=	Fourier series coefficient
C_d	=	drag coefficient for wave force
C_m	=	inertial coefficient for wave force
C_n	=	Fourier series coefficient
[C]	=	global damping matrix
$[C]_H$	=	hydrodynamic damping matrix of riser system
$[C]_M$	=	equivalent viscous damping matrix of riser system
d	=	water depth
D	=	effective diameter for wave force calculation
D_n	=	Fourier series coefficient
$D(\bullet)$	=	directional spreading function
E	=	riser modulus of elasticity
$E(w)$	=	unidirectional wave energy spectrum
$E(w, \bullet)$	=	directional wave energy spectrum
$E(w_j, \bullet_j)$	=	the wave energy at frequency w_j and direction \bullet_j
f	=	total force per unit length on the riser
f_{drag}	=	drag force per unit length on the riser

$\{F\}$	= global force array on riser
g	= acceleration due to gravity
h	= distance above seabed
H	= wave height
H_n	= n^{th} cubic Hermitian polynomial function
H_s	= significant wave height
i	= $\sqrt{-1}$
I	= riser moment of inertia
k	= wave number
k_{ij}	= i^{th} row and j^{th} column of $[k]_{TOT}$
$[k]_{EI}$	= element bending stiffness matrix
$[k]_{T_o}$	= element constant tension stiffness matrix
$[k]_{T_v}$	= element varying tension stiffness matrix
$[k]_{TOT}$	= total stiffness matrix of element
$[K]$	= global stiffness matrix of riser system
KE	= kinetic energy
L	= length of element
$[m]_{TOT}$	= total mass matrix of element
m	= steel mass plus mud mass per unit length
m_a	= added mass per unit length
m_o	= volume under the directional wave energy spectrum or area under the unidirectional wave energy spectrum
M	= moment along the riser
$[M]$	= global mass matrix of riser system
N	= number of modes

- ρ = mass density of sea water
 rms = root mean square
 R = radius of curvature along the riser
 R_{sig} = significant peak-to-peak riser displacement
 s = concentration factor
 SE = strain energy
 S_x = volume under the directional displacement spectrum
 t = time
 $TF(\omega_j, \phi_j)$ = transfer function of riser system at frequency ω_j
 and direction ϕ_j
 T = effective tension along riser
 T_0 = initial constant effective tension at $z=0$ of element
 T' = varying tension per unit length along riser
 u_c = current velocity
 u_w = wave particle velocity
 \dot{u}_w = wave particle acceleration
 u_0 = amplitude of wave particle velocity
 V = wind speed 64 feet above sea surface (ft/sec)
 w = wave frequency in rads/sec
 ω_{n_i} = natural frequency of mode i in rads/sec
 y_i = nodal displacements and rotations for an element
 y_0 = complex riser response of form $a + bi$
 \ddot{y} = riser acceleration
 \dot{y} = riser velocity
 y = riser displacement
 \bar{y} = distance from neutral axis to outer edge of riser

- z = vertical coordinate along length of riser element
 $!$ = factorial
 β_i = modal damping parameter(% of critical/100) for mode i
 δ_{ij} = Kronecker delta function ≈ 1 for i equal to j
 ≈ 0 for i not equal to j
 $[\Phi]$ = the *normalized modal matrix* obtained from the eigen analysis
 $\{\phi_i\}$ = normalized eigenvector for mode i
 θ = phasing angle
 π = pi
 σ = bending stress along the riser
 Γ = gamma function
 \bullet = angle about the mean peak direction
 $\bar{\bullet}$ = angle of mean peak direction
 $()'$ = $d()/dz$

VITA

Gerard Lewis McCoy III was born in White Plains, New York, on December 5, 1959. He spent most of his childhood in lower New York state before graduating from Byram Hills High School in Armonk, New York, in June, 1977. In August, 1977, Gerard entered Texas A & M University in the ocean engineering program. He received his B.S. degree in May, 1982, and entered graduate school at Texas A & M University the following August, again in the ocean engineering program. During graduate school he was employed as a half-time research assistant working on a manganese nodule mining project.

Gerard can be reached through his parents:

Mr. and Mrs. Gerard L. McCoy, Jr.

P.O. Box 538

7 Fairmount Rd.

Goldens Bridge, New York 10526